

Supporting Information

Networking hole and electron hopping paths by Y-shape host molecules: Promoting blue phosphorescence organic light emitting diodes

Jau-Jiun Huang,^a Lik-Ka Yun,^b Te-Jen Kung,^b Chi-Lin Chen,^a Jiun-Haw Lee,^{*b} Yuh-Renn Wu,^b Tien-Lung Chiu,^{*c} Pi-Tai Chou,^a and Man-kit Leung^{*a}

a. Department of Chemistry, National Taiwan University, 1 Roosevelt Road Section 4, Taipei 106, Taiwan, R.O.C. E-mail: mkleung@ntu.edu.tw

b. Graduate Institute of Photonics and Optoelectronics and Department of Electrical Engineering, National Taiwan University, 1 Roosevelt Road Section 4, Taipei 106, Taiwan, R.O.C. Email: jiunhawlee@ntu.edu.tw

*c. Department of Photonics Engineering, Yuan Ze University, 135 Yuan-Tung Road, Taoyuan 32003, Taiwan, R.O.C. *Email: tlchiu@saturn.yzu.edu.tw*

List of supporting information

	page
Fig. S1 The stacking structure of TCbzBz .	3
Fig. S2 TGA measurement of TCbzBz .	4
Fig. S3 DSC measurement. The DSC scanning of (a) DCbzBz and (b) the sublimed TCbzBz .	5
Fig. S4 The overlapped spectra of (a) UV-vis absorption and (b) LTPH for comparison.	6
Fig. S5 The occupied MO levels for TCbzBz and their spatial distributions calculated by DFT calculation is based on DFT/B3LYP/6-31+g**.	7
Fig. S6 The unoccupied MO levels for TCbzBz and their spatial distributions calculated by DFT calculation is based on DFT/B3LYP/6-31+g**.	7
Fig. S7 The occupied MO levels for DCbzBz and their spatial distributions calculated by DFT calculation is based on DFT/B3LYP/6-31+g**.	8
Fig. S8 The unoccupied MO levels for DCbzBz and their spatial distributions calculated by DFT calculation is based on DFT/B3LYP/6-31+g**.	8
Table S1 Absorption wavelength (lcal), oscillator strength (f) and transition character of DCbzBz calculated by TD/DFT/B3LYP/6-311+g**.	9
Table S2 Absorption wavelength (lcal), oscillator strength (f) and transition character of TCbzBz calculated by TD/DFT/B3LYP/6-311+g**.	9

Fig. S9 The time-dependent fluorescence decay experiments with excitation wavelength of 310 nm.	10
Fig. S10 CV and DPV for (a) oxidation and (b) reduction scanning of TCbzBz .	10
Fig. S11 (a) The photoelectron spectrometer of TCbzBz measured with 50-nm thin-film and (b) its absorption with simulation curves.	11
Fig. S12 The distributions of DOS for HOMO and LUMO level which obtained by simulation.	11
Fig. S13 The simulation curves for (a) HOD and (b) EOD.	12
Scheme S1 The HOMO/LUMO levels in the EL devices and the corresponding chemical structures.	13
Fig. S14 The EL performances for TCbzBz based device A1, A2, A3 and A4.	14
Table S3 EL Characteristics of various PhOLEDs Devices.	15
Fig. S15. Comparison of the UV-Vis absorption spectra of DCbzbz (left) and TCbzbz (right) in a THF solution and in a vacuum deposited film	16
Fig. S16. Comparison of the powder X-ray diffractograms of TCbzbz in a vacuum deposited film (top) and in crystalline solid (bottom).	17
Fig. S17. Comparison of the atomic force microscopic image of vacuum deposited films of DCbzbz (top) and TCbzbz (bottom): (a) scan topography (left) and (b) phase images (right).	18
Fig. S18 ¹ H spectrum of compound 1 in CD ₂ Cl ₂	20
Fig. S19 ¹³ C spectrum of compound 1 in CD ₂ Cl ₂	20
Fig. S20 ¹ H spectrum of TCbzBz in CD ₂ Cl ₂	21
Fig. S21 ¹³ C spectrum of TCbzBz in CD ₂ Cl ₂	21
References	22

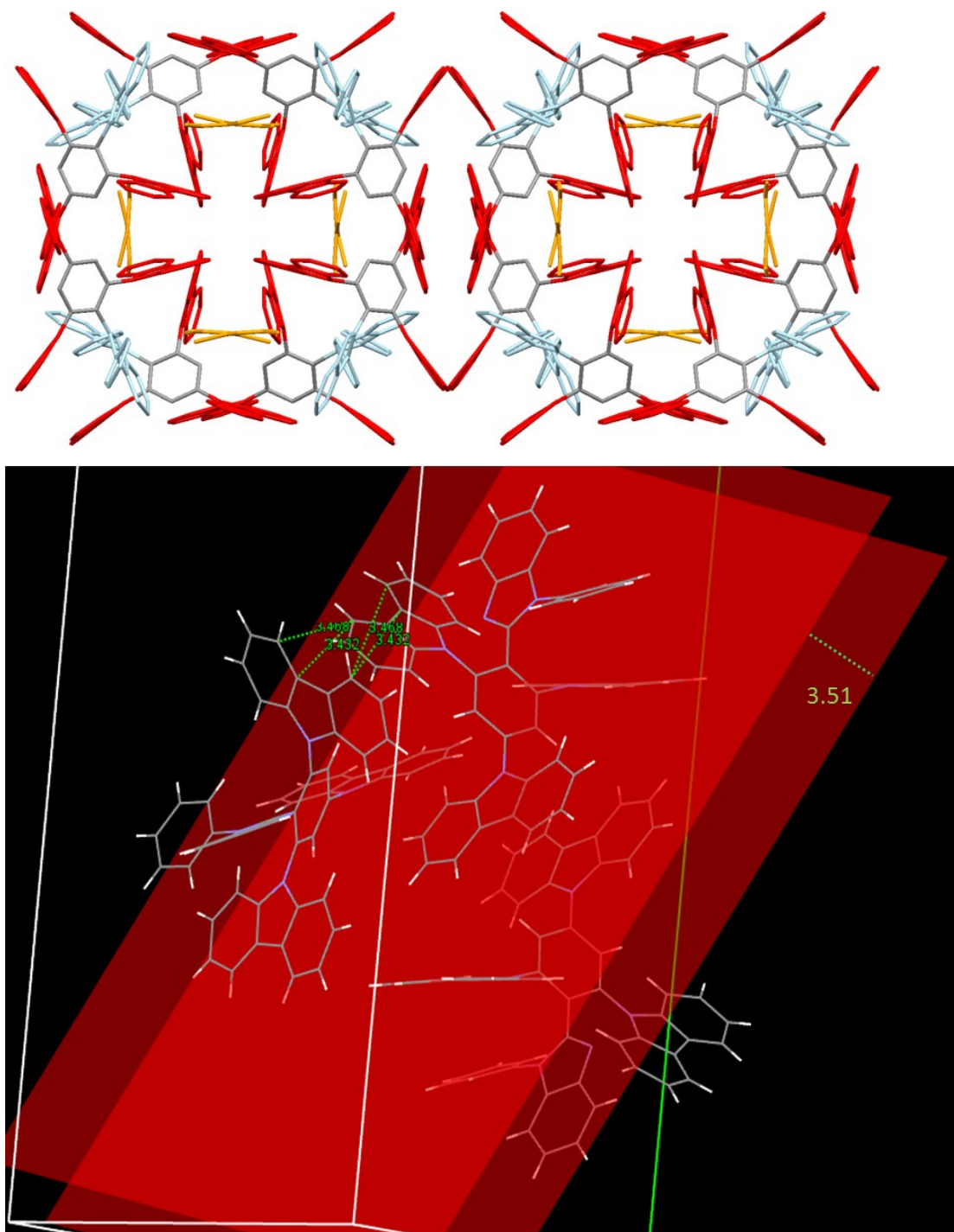


Fig. S1 (Top)The stacking structure of **TCbzBz** was observed to contain an additional sixteen EtOAc molecules per unit cell, where Cbz and Bz units are labelled with red and light blue color, and EtOAc molecules are denoted orange color. (Bottom) Two groups of close contact carbazole substituents can be identified. One group is almost parallel with the inter-plane distance of 3.51 Å. The other group is tilted to each other, with a closest C-C distances of 3.432 and 3.468 Å.

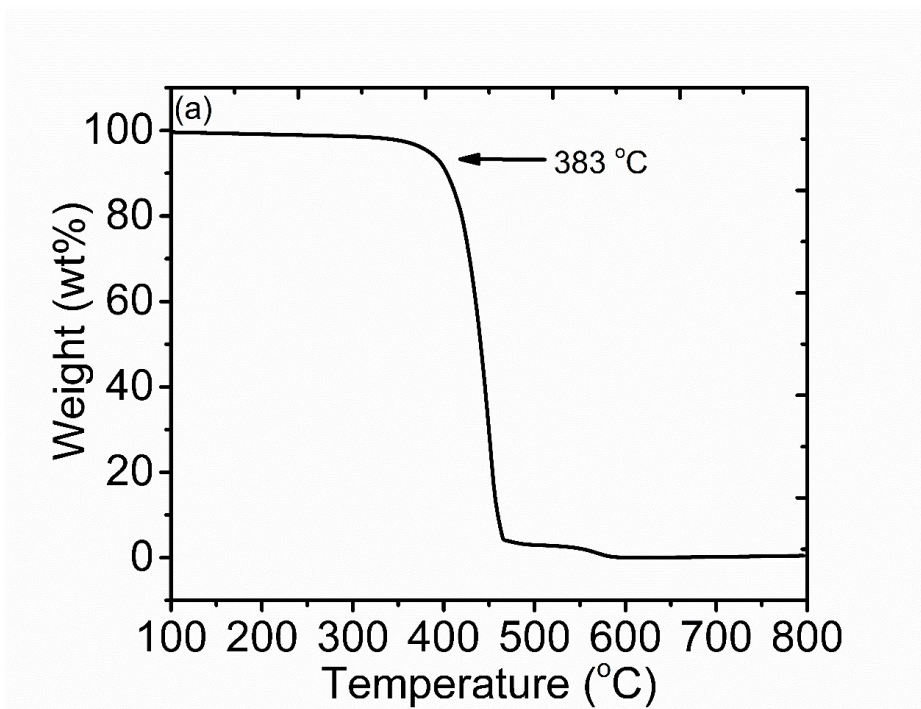


Fig. S2 TGA measurement of **TCbzBz**. The temperature was held at 110.0 °C for 10.0 min and then further heated from 110.0 °C to 800.0 °C with a heating rate 10.0 °C/min under nitrogen atmosphere.

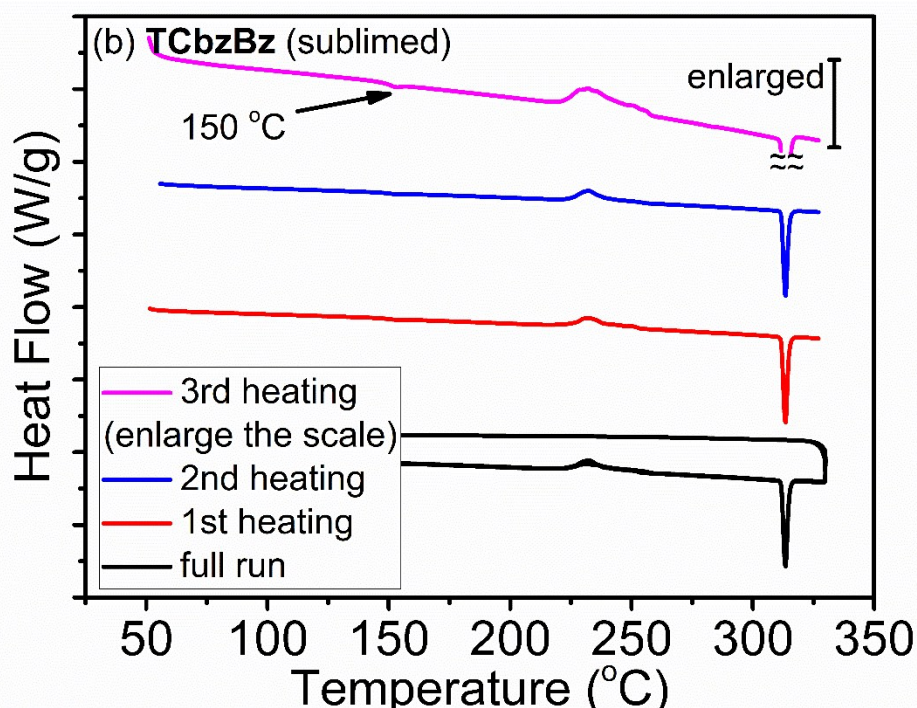
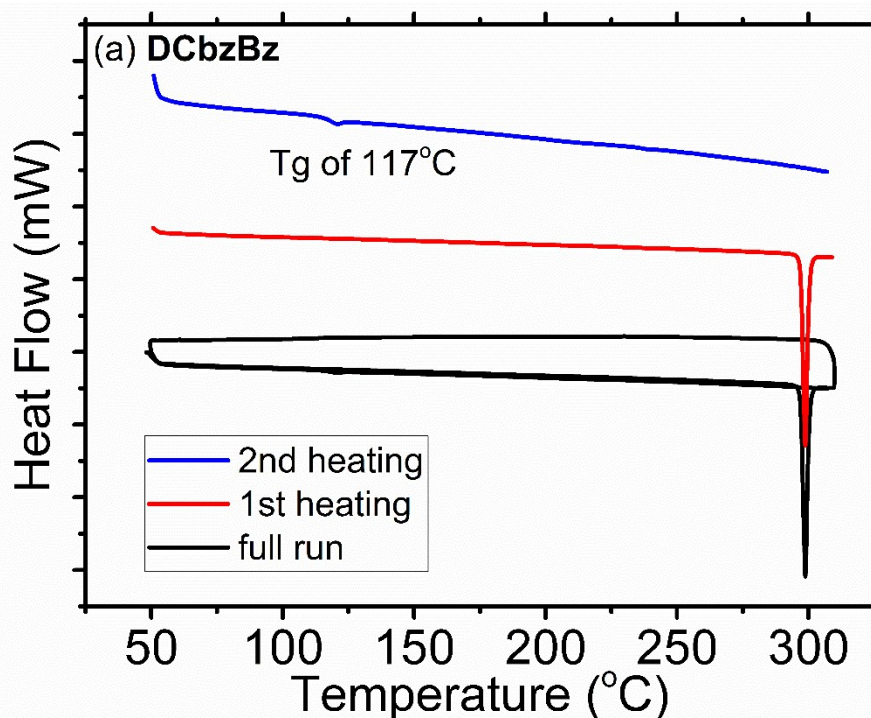


Fig. S3 DSC measurement. The DSC scanning of (a) **DCbzBz** and (b) the sublimed **TCbzBz**. The temperature was preheated to the desired temperature with rate of 10.0 °C/min and held on at the temperature for 10 minutes in the first round to ensure that the compounds entirely are melting. The sample was then cooled to 50.0 °C with a cooling rate of 20.0 °C/min. In the second and third heating round, the temperature was raised with a heating rate of 10 °C/min.

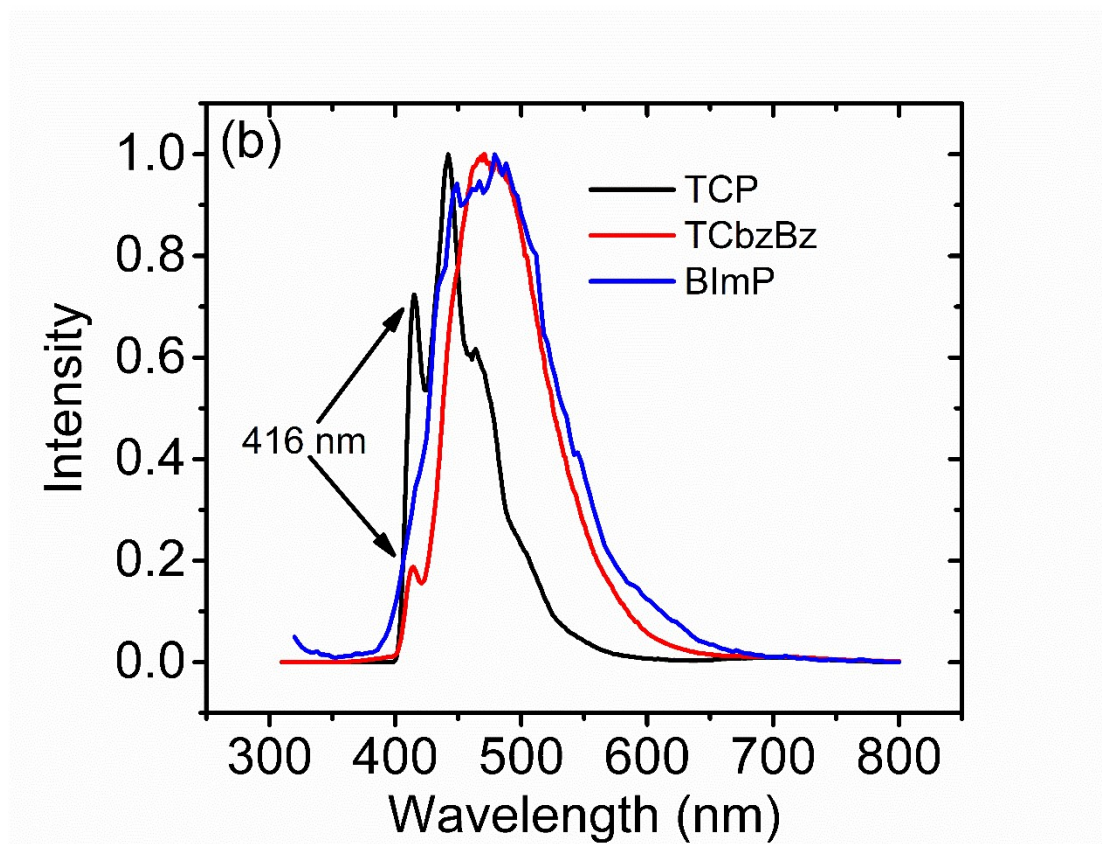
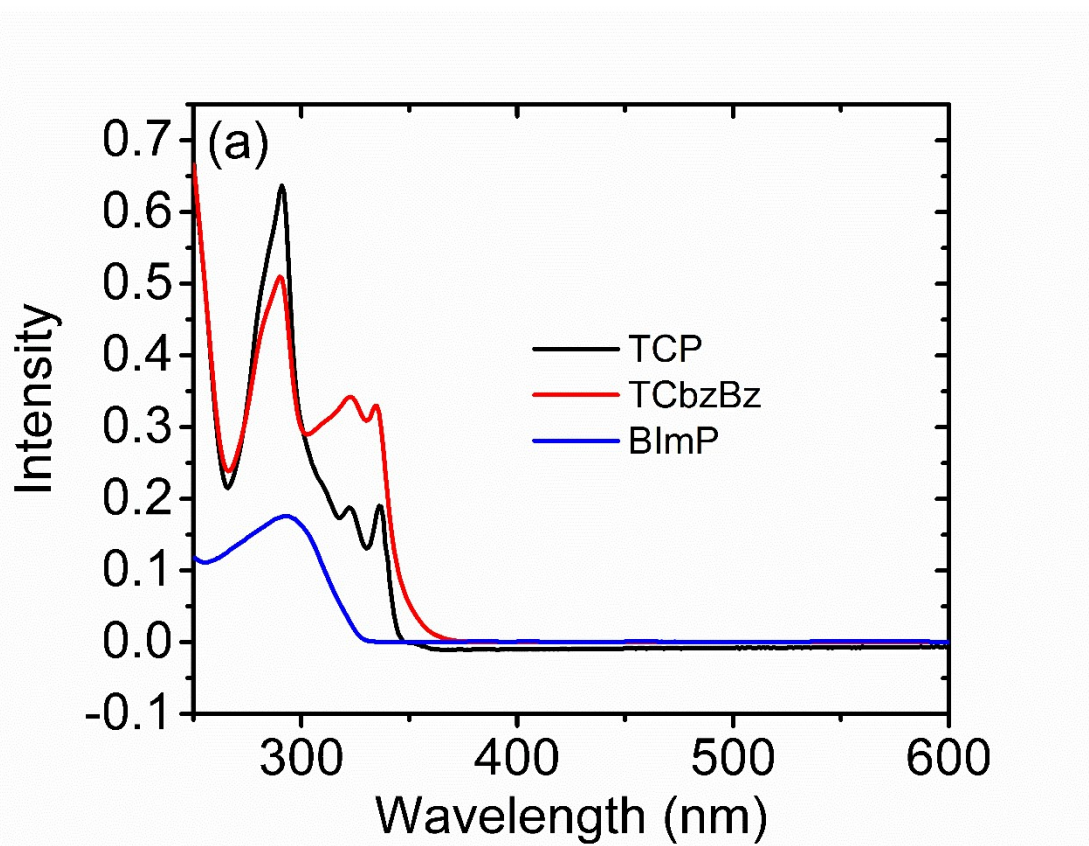


Fig. S4 The overlapped spectra of (a) UV-vis absorption and (b) LTPH for comparison.

Fig. S5 The occupied MO levels for **TCbzBz** and their spatial distributions calculated by DFT calculation is based on DFT/B3LYP/6-31+g**

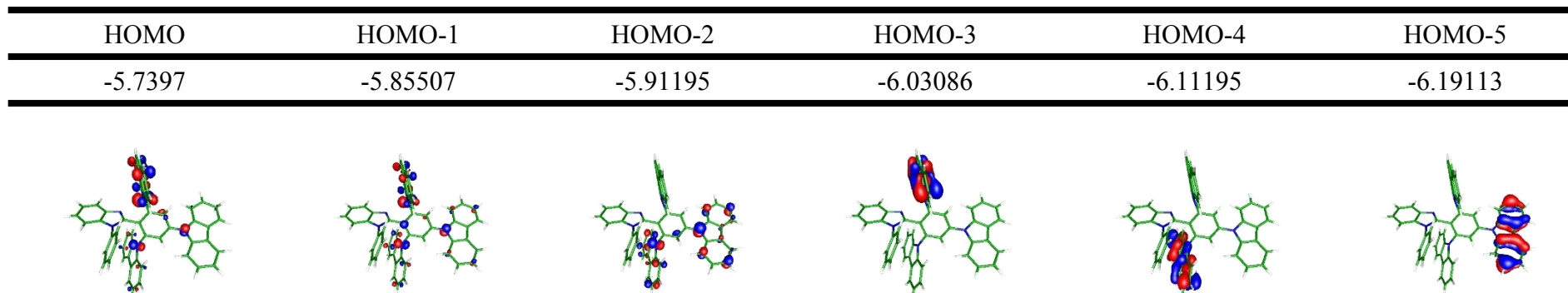


Fig. S6 The unoccupied MO levels for **TCbzBz** and their spatial distributions calculated by DFT calculation is based on DFT/B3LYP/6-31+g**

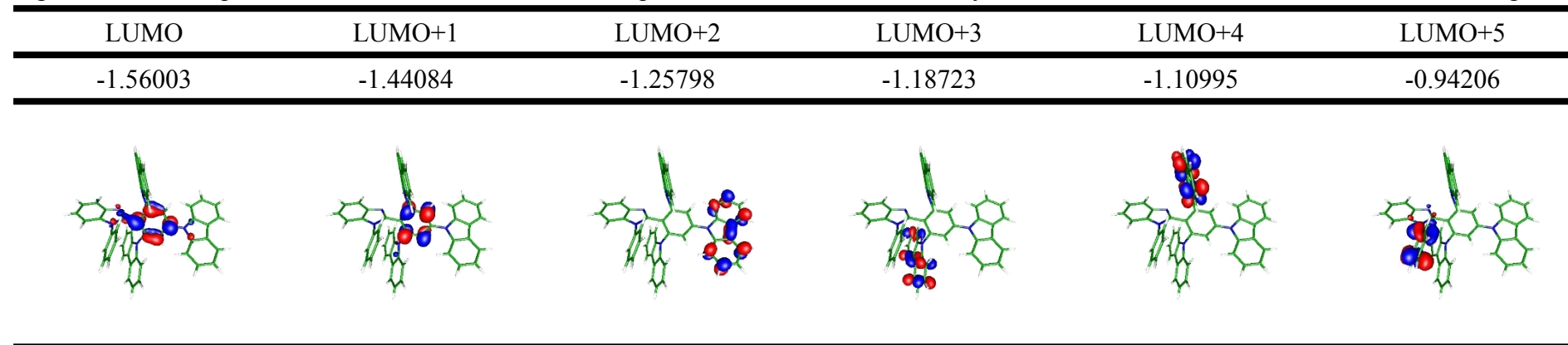


Fig. S7 The occupied MO levels for **DCbzBz** and their spatial distributions calculated by DFT calculation is based on DFT/B3LYP/6-31+g**

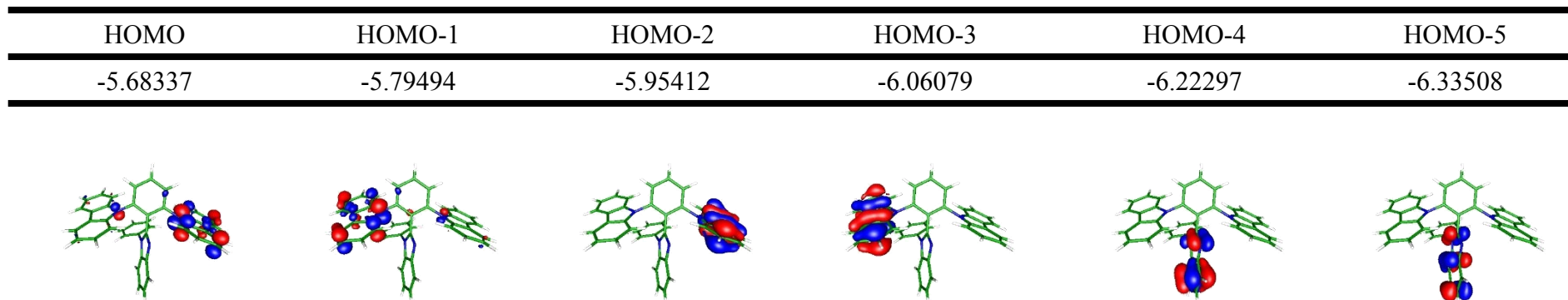


Fig. S8 The unoccupied MO levels for **DCbzBz** and their spatial distributions calculated by DFT calculation is based on DFT/B3LYP/6-31+g**

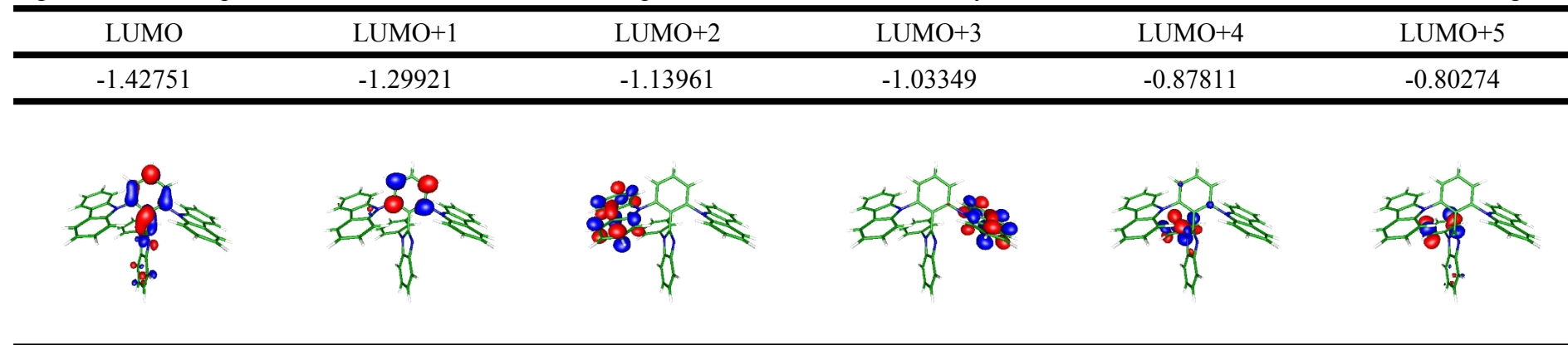


Table S1 Absorption wavelength (λ_{cal}), oscillator strength (f) and transition character of **DCbzBz** calculated by TD/DFT/B3LYP/6-311+g**. (Abbreviations: H, HOMO. L, LUMO. H-1, HOMO-1, L+1, LUMO+1, etc.)

State	λ_{cal} (nm)	f	Transition character
S ₁	347.36	0.0111	H→L (95%), H→L+1 (4%)
S ₂	335.52	0.0249	H-1→L (65%), H→L (3%), H→L+1 (32%)
S ₃	330.79	0.0061	H-1→L (35%), H→L (3%), H→L (62%)
S ₄	324.03	0.0246	H-1→L+1
S ₅	313.48	0.023	H-2→L (85%), H→L+3 (15%)

Table S2 Absorption wavelength (λ_{cal}), oscillator strength (f) and transition character of **TCbzBz** calculated by TD/DFT/B3LYP/6-311+g**. (Abbreviations: H, HOMO. L, LUMO. H-1, HOMO-1, L+1, LUMO+1, etc.)

State	λ_{cal} (nm)	f	Transition character
S ₁	353.38	0.0411	H-1→L (2%), H→L (89%), H→L+1 (8%)
S ₂	342.66	0.0161	H-1→L (11%), H→L (10%), H→L+1 (79%)
S ₃	338.04	0.024	H-2→L (6%), H-1→L (70%), H-1→L+1 (7%), H→L+1(15%)
S ₄	333.19	0.1599	H-2→L (65%), H-2→L+1(10%), H-1→L+1(25%)
S ₅	313.48	0.023	H-2→L (23%), H-2→L+1 (3%), H-1→L (15%), H-1→ L+1 (59%)

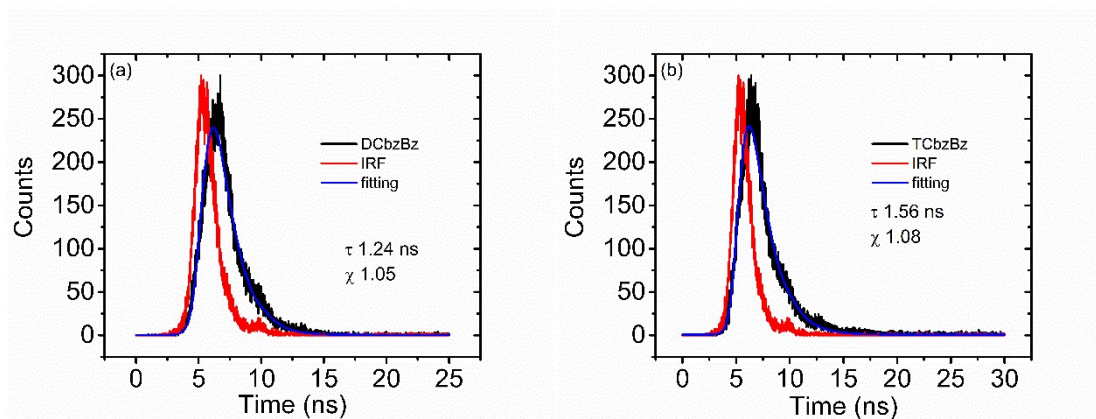


Fig. S9 The time-dependent fluorescence decay experiments with excitation wavelength of 310 nm.

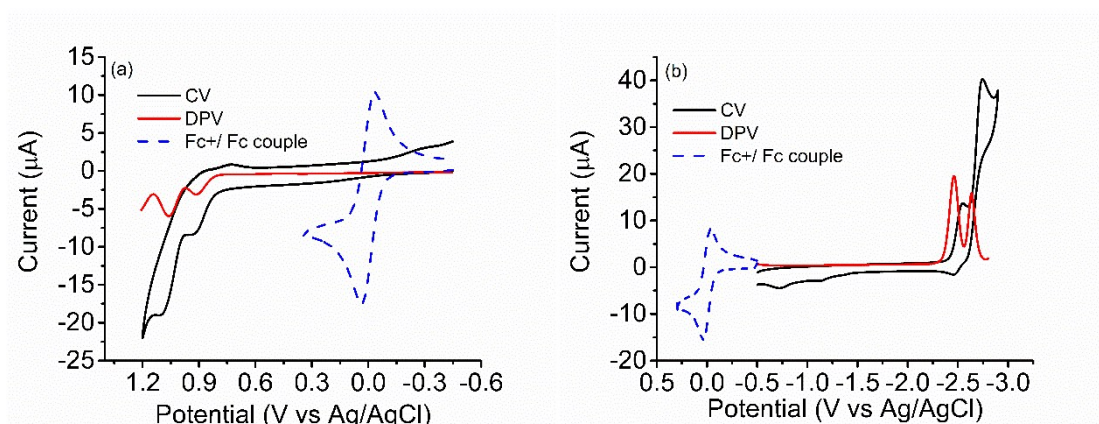


Fig. S10 CV and DPV for (a) oxidation and (b) reduction scanning of **TCbzBz**. The oxidation and reduction were measured in MeCN and dried DMF with 10^{-3} M, respectively. The Pt working electrode was used for oxidation scanning and glassy carbon working electrode was employed for reduction scanning. The supporting electrolyte is tetrabutylammonium perchlorate (0.1 M). The scan rate was 100 mV/s. The HOMO and LUMO levels were estimated according to Forrest approach.^{1,2} $E_{\text{HOMO}} = -(1.4 \pm 0.1) \times (q \times E_{\text{DPV}}) + (-4.6 \pm 0.08)$ eV, and $E_{\text{LUMO}} = (-0.92) \times (q \times E_{\text{DPV}}) + (-4.6 \pm 0.08)$ eV, in here q is +1. The E_{DPV} for oxidation and reduction scanning were recorded as 0.9 and -2.45 V with Fc/Fc⁺ used as internal standard, respectively. Consequently, the HOMO and the LUMO levels are -5.86 ± 0.08 and -2.34 ± 0.08 eV.

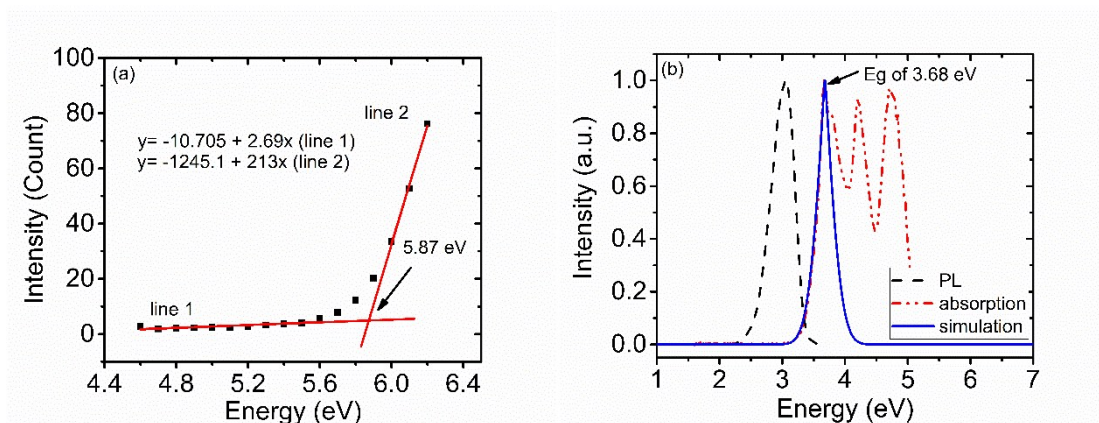


Fig. S11 (a) The photoelectron spectrometer of **TCbzBz** measured with 50-nm thin-film and (b) its absorption with simulation curves. The energy gap (E_g) of 3.68 eV was estimated by the lowest absorption λ_{\max} . Therefore, the HOMO/LUMO levels were found to be 5.87/2.19 eV according to equation $E_{\text{LUMO}} = E_{\text{HOMO}} + E_g$, respectively.

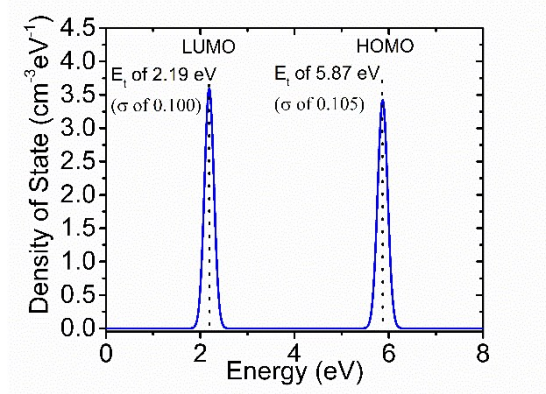


Fig S12 The distributions of DOS for HOMO and LUMO level which obtained by simulation.

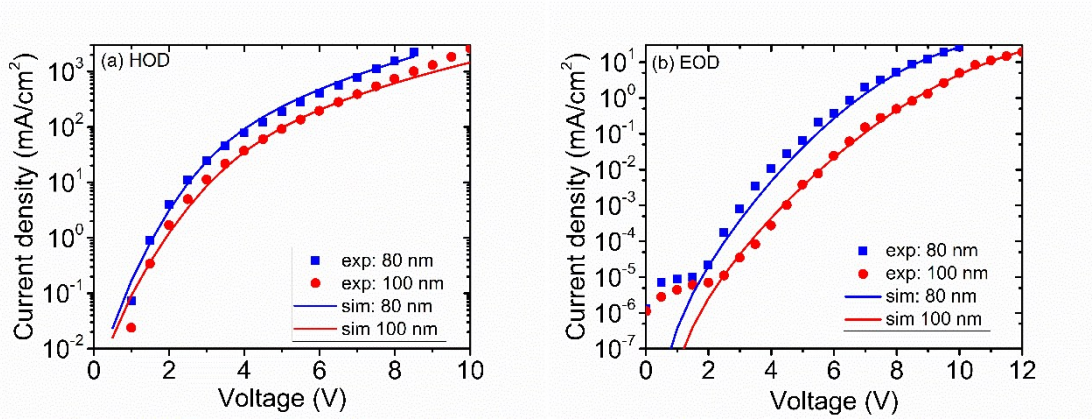
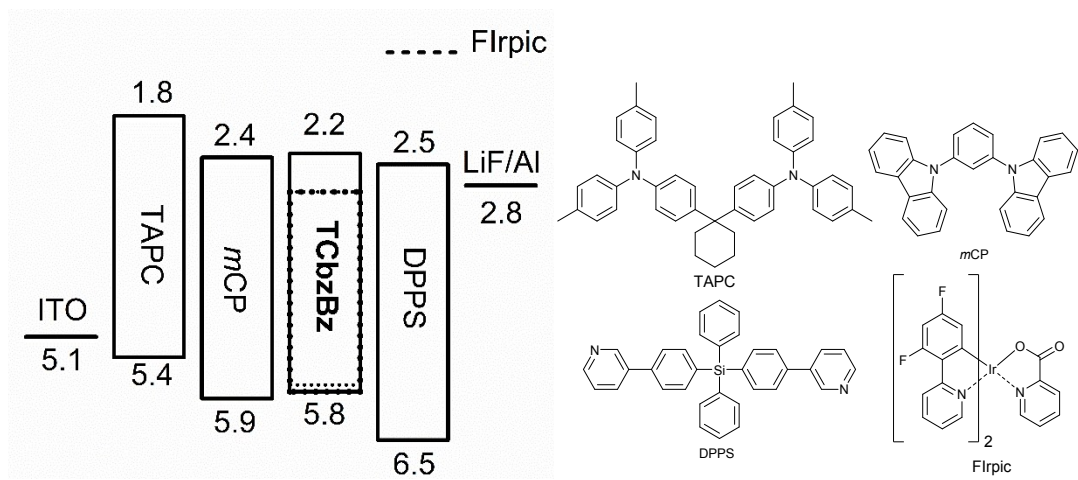


Fig S13 Simulation curves for (a) HOD and (b) EOD. A configuration of ITO/Al (50 nm)/MoO₃ (10 nm)/mCP (5 nm)/TCbzBz (80 and 100 nm)/mCP (5 nm)/MoO₃ (10 nm)/Al (100 nm) for the HODs and a configuration of glass/Al (50 nm)/LiF (1 nm)/DPPS (5 nm)/TCbzBz (80 and 100 nm)/DPPS (5 nm)/LiF (1 nm)/Al (100 nm) for the EODs were used. Securing the simulation to be feasible, the single-carrier devices were fabricated with two different thicknesses of 80 nm and 100 nm for host layer. We made an attempt to substitute various carrier mobility (μ), factor of the field dependence (β) values and the Gaussian distribution of DOS into Poisson-drift-diffusion solver, and then find out the J-V curve that fits the experimental curve. Next, the zero-field mobility (μ_0) can be afforded by employing Poole-Frenkel equation $\mu = \mu_0 \times \exp(\beta\sqrt{E})$.



Scheme S1 The HOMO/LUMO levels in the EL devices and the corresponding chemical structures.

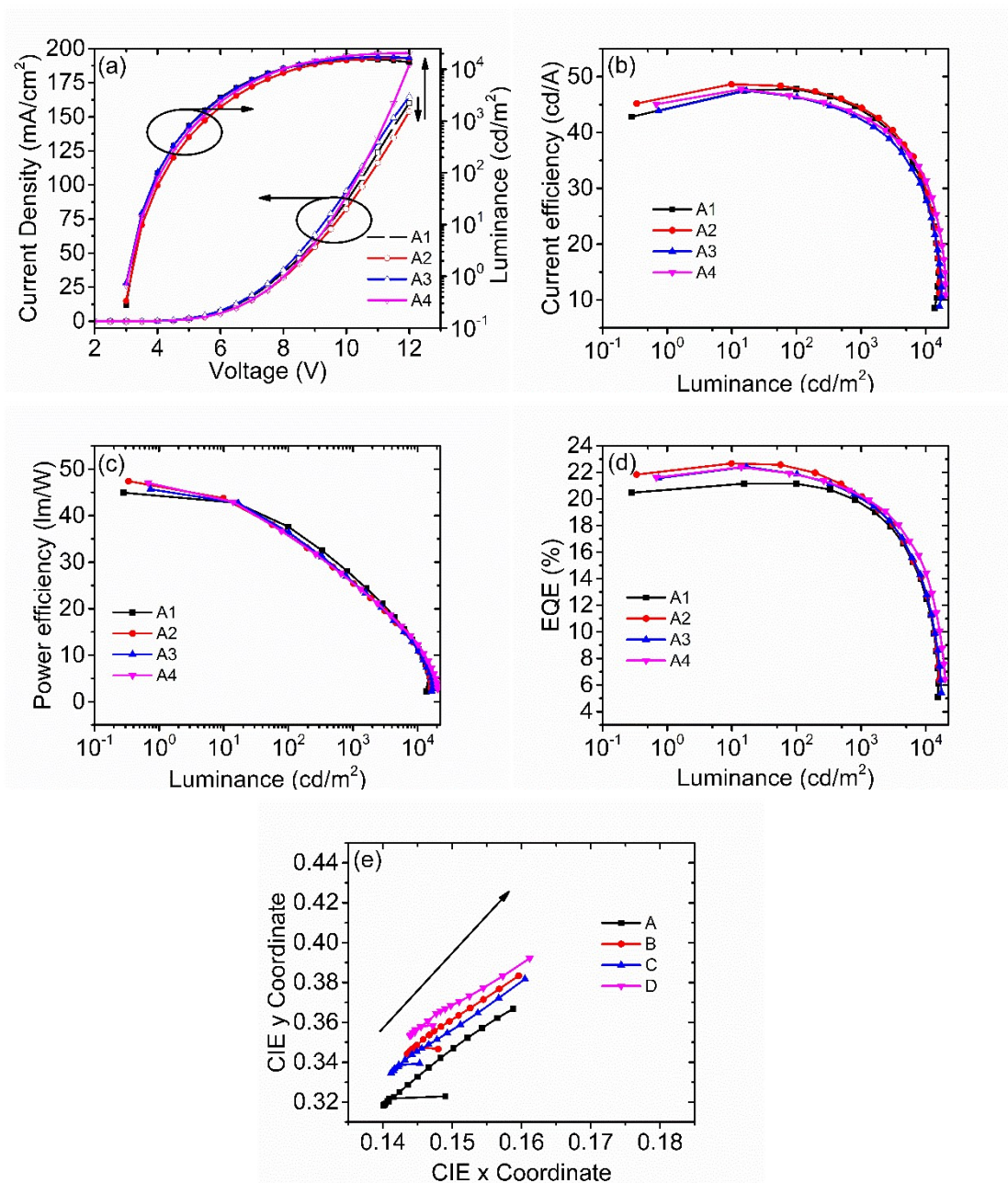


Fig. S14 The EL performances for TCbzBz based device A1, A2, A3 and A4 with configuration of indium tin oxide / TAPC (4,4'-cyclohexylidenebis[N,N-bis(4-methylphenyl)benzenamine]) (50 nm)/ mCP (10 nm)/ hosts: x wt% FIrpic (30 nm)/ DPPS (30 nm)/ LiF (0.9 nm)/ Al (120 nm). Device A1, A2, A3, and A4 represents 3%, 6%, 9% and 12% FIrpic, respectively. (a) $J-V-L$ curves; (b) CE versus luminance curves; (c) PE versus luminance curves; (d) EQE versus luminance curves and (e) CIE coordinate.

Table S3 EL Characteristics of various PhOLEDs Devices

Device	V_{on} (V) ^a	L_{max} (cd/m ²)	CE (cd/A) ^b	PE (lm/W) ^b	EQE (%) ^b	CIE ($\Delta x, \Delta y$) ^c
A1	3.0	15620	47.8, 44.6, 37.5	45.0, 28.1, 18.1	21.2, 19.9, 16.7	(0.008, 0.002)
A2	3.0	16310	48.7, 44.4, 37.8	47.4, 29.0, 19.5	22.7, 20.2, 16.8	(0.003, 0.002)
A3	3.0	17500	47.5, 43.0, 36.4	45.7, 27.0, 17.5	22.4, 20.4, 17.0	(0.003, 0.0003)
A4	3.0	20570	47.7, 42.3, 35.9	47.0, 27.6, 16.2	22.4, 20.0, 16.8	(0.002, 0.003)

a. V_{on} : turn-on voltage is defined at 1 cd m⁻²; b. Recorded at maximum, 1000 and 5000 cd m⁻², respectively; c. In the range from the minimum luminance to 5000 cd/m².

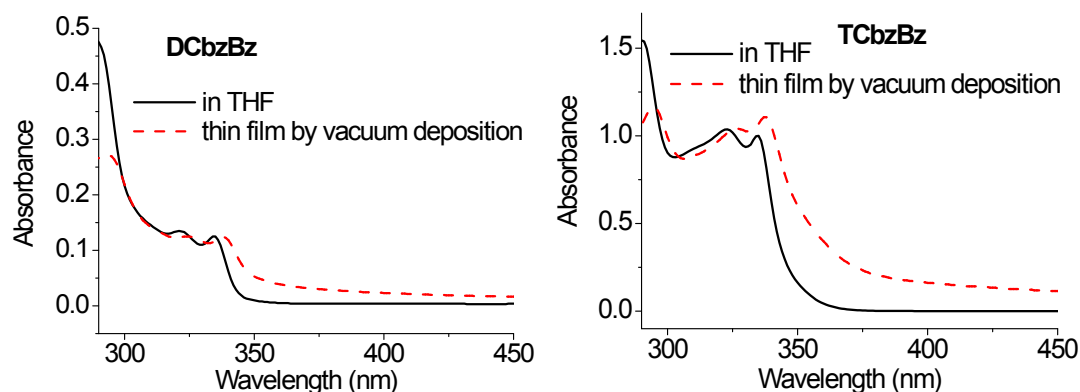


Fig. S15. Comparison of the UV-Vis absorption spectra of **DCbzBz** (left) and **TCbzBz** (right) in a THF solution and in a vacuum deposited film.

To probe the intermolecular interactions of the host molecules in solid state, we have subjected the hosts to UV-vis absorption spectral analysis. Figure Fig. S19 compares the absorption spectra of **DCbzBz** in solid sublimed film and in solution. The vibronic bands peaking at 322 and 334 nm in the range of about 300-350 nm are typical electronic π - π^* transitions of the carbazole moieties. The pattern is very similar to that of the ${}^1L_b \rightarrow {}^1A$ ($S_1 \rightarrow S_0$) transitions of a carbazole molecule, in which the transition dipole is parallel to its short axis. Although bathochromic shift of the absorption bands (λ_{\max} : 326 and 338 nm) are observed, the spectral pattern and their relative intensities are almost identical in two cases, indicating that the intermolecular stacking in the solid film is insignificant and the film can be considered as amorphous.

On the other hand, **TCbzBz** exhibits not only a bathochromic shift, from 322, 334 nm to 326, 337 nm, but also a significant change in their relative intensities. Similar to the observed phenomenon in the micro-crystals of carbazole,³ the absorption of solid **TCbzBz** film at 338 nm is largely enhanced in comparison to **TCbzBz** in solution. These results reflected **TCbzBz** does have high tendency towards aggregation in solid film, like carbazole in micro-crystals. Noteworthy to mention is that carbazole molecules in a single crystal are aligned in a head-to-tail fashions, with the molecules in the unit cell closely packed in a herring bond array.⁴ This is consistent with our observation in the single crystal crystallographic analysis, which shows antiparallel pairs of the carbazole segments with a short spatial distance of 3.67Å. This is unusual because one may usually assume an amorphous morphology in a sublimed film.

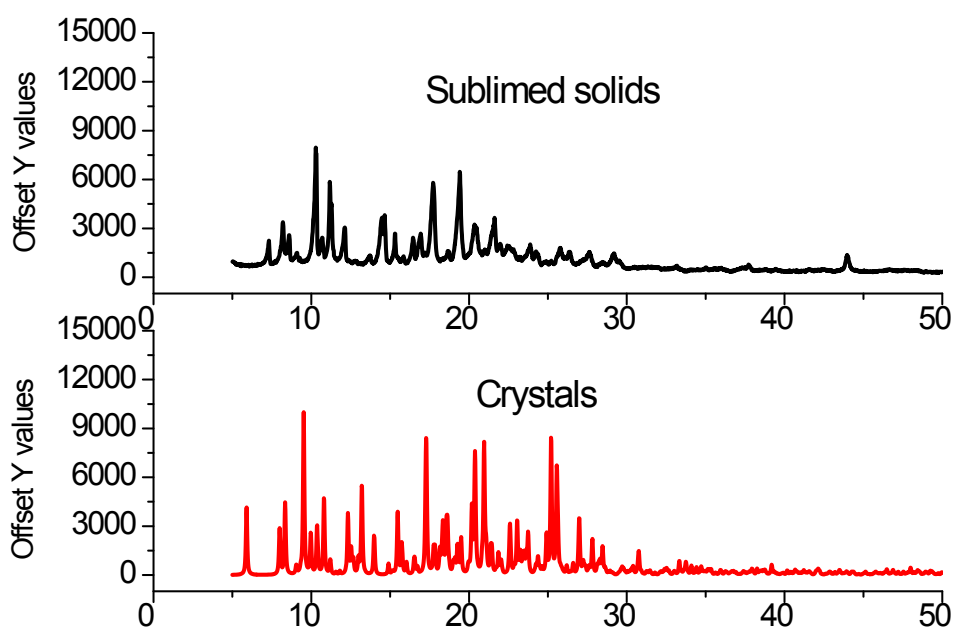


Fig. S16. Comparison of the powder X-ray diffractograms of **TCbzbz** in a vacuum deposited film (top) and in crystalline solid (bottom).

To further elucidate the aggregation of **TCbzbz** in solid film, we have subjected the sublimed **TCbzbz** sample for powder X-ray analysis. Sharp and strong diffraction bands are illustrated in Fig. S20, indicating that high crystallinity does exist in the sublimed sample. However, due to the lost of the EtOAc molecules, the obtained diffraction pattern is no longer identical with that from the single crystals.

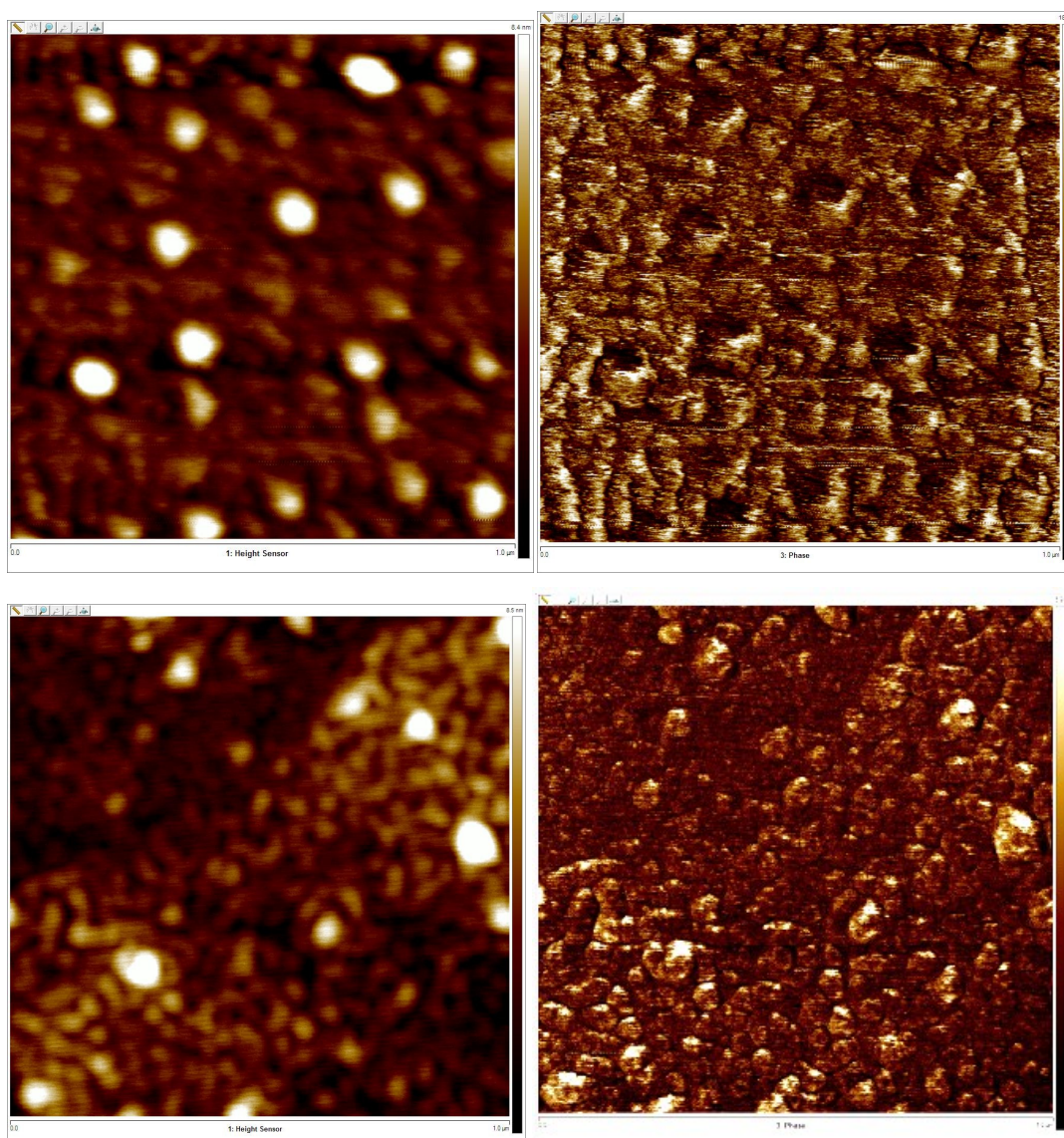


Fig. S17. Comparison of the atomic force microscopic image of vacuum deposited films of **DCbzbz** (top) and **TCbzbz** (bottom): (a) scan topography (left) and (b) phase images (right).

The method of atomic force microscopy (AFM, Veeco BioScope) was employed to investigate the surface morphologies of the vacuum deposited **DCbzbz** and **TCbzbz** thin films on a polished silicon wafer. To prevent the inaccuracy from contact damages, we used the low noise tapping mode to scan topography and phase images of these films. Tapping mode is known for imaging soft samples such as polymers or organic materials. This method not only allows us to study the topography of the film surface but also to detect the heterogeneity in the tribological surface caused by the presence of various phases in the films. Figure S21 shows the AFM image (1 mm × 1 mm) of **DCbzbz** and **TCbzbz** obtained by scan topography mode (left) and phase images

(right). Similar surface roughness can be seen in both cases. However, drastic differences can be seen in the phase images; while homogeneous texture can be found in the image of **DCbzbz** (right, top), indicating the deposited film is amorphous, nano-granules can clearly be observed in image of **TCbzbz**. The domain sizes of 10-100 nm can roughly be estimated. This observation strongly suggests that high crystallinity does exist in the vacuum deposited film of **TCbzbz**.

In summary, our evidences suggest that the solid state morphology of **TCbzbz** is completely different from that of **DCbzbz**. Strong aggregation tendency can clearly be seen. Formation of nano-granules on one hand would allow effective charge transport within the granule. On the other hand, tight packing of the nano-granules would allow charge hopping between the nano-granules.

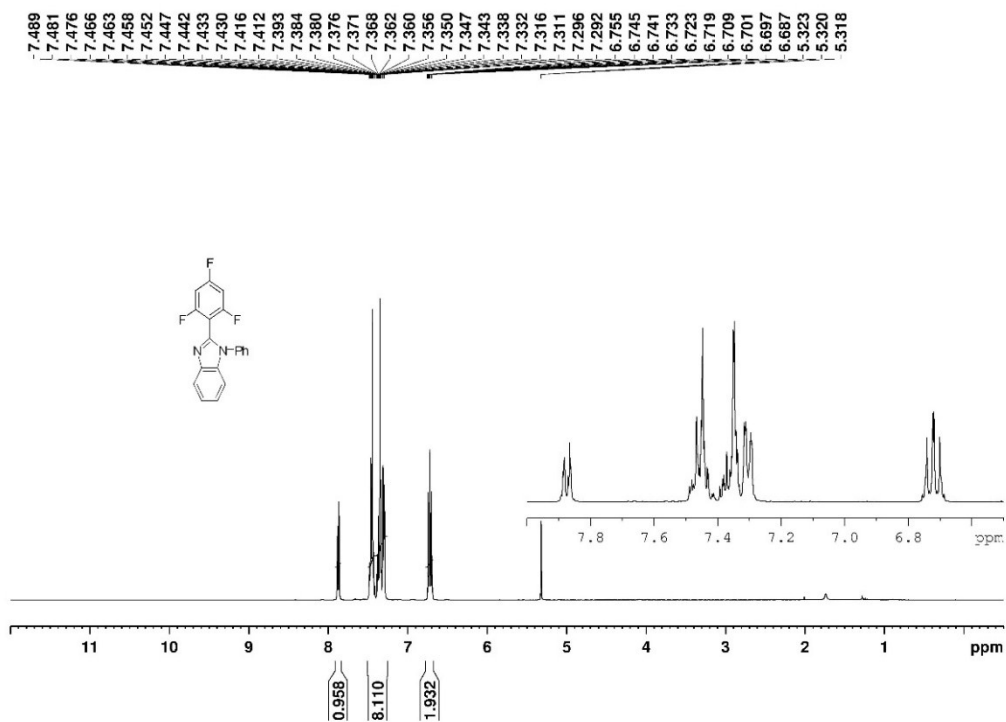


Fig. S18 ¹H NMR spectrum of compound **1** in CD₂Cl₂

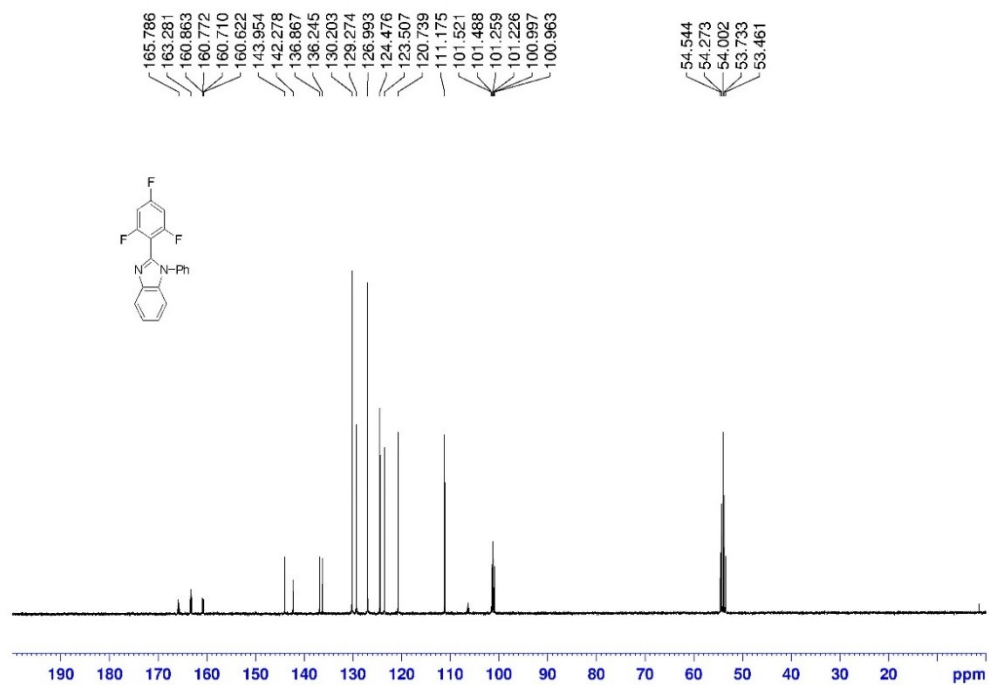


Fig. S19 ¹³C NMR spectrum of compound **1** in CD₂Cl₂

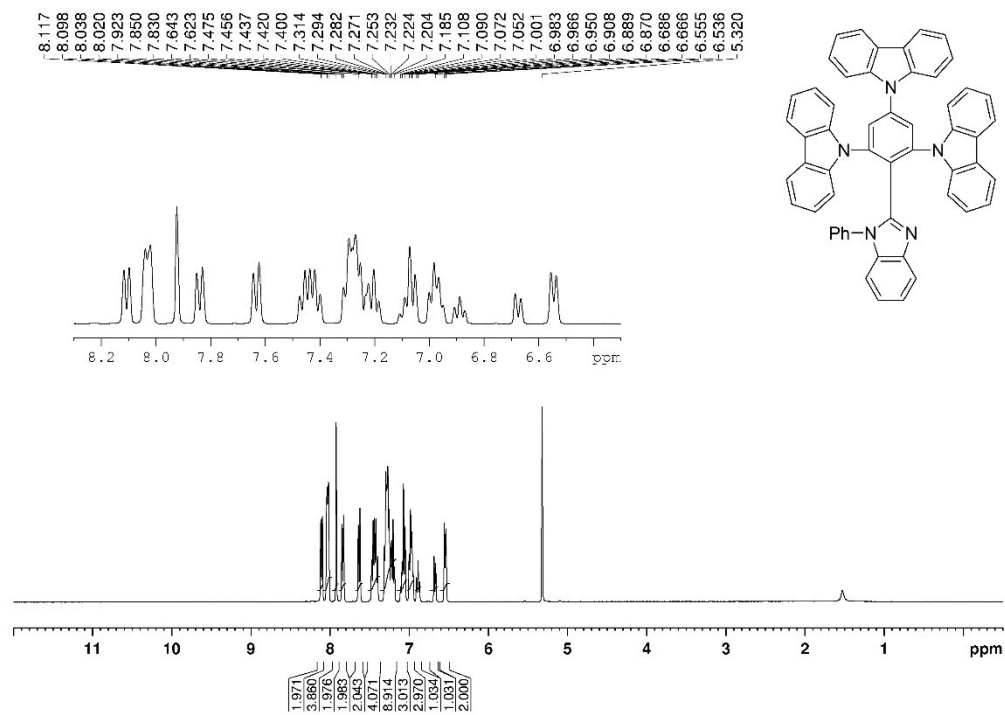


Fig. S20 ¹H NMR spectrum of TCbzBz in CD₂Cl₂

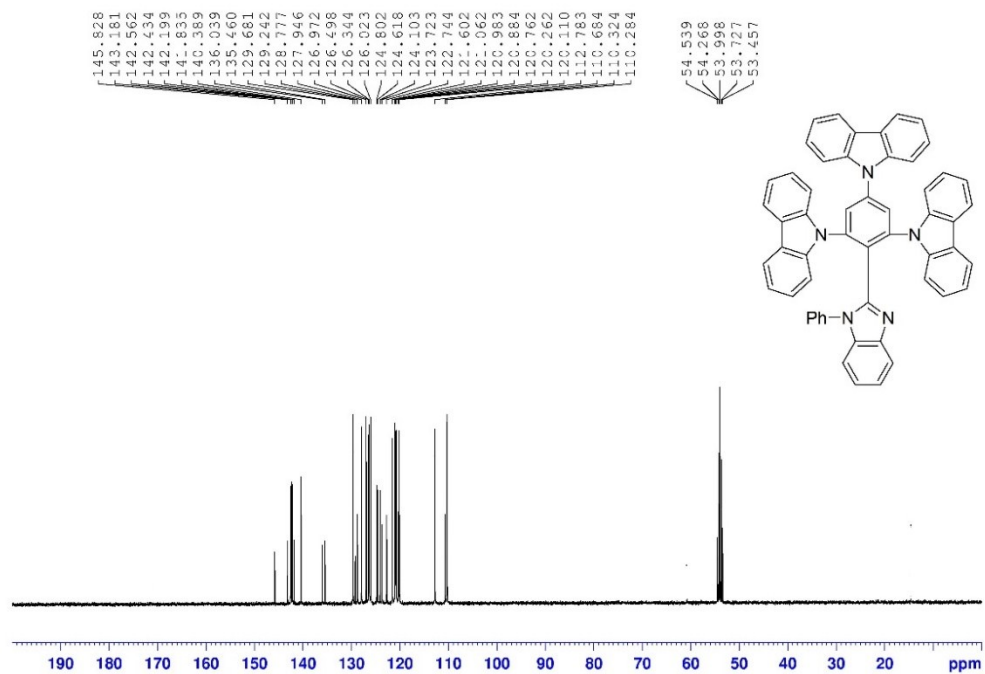


Fig. S21 ¹³C NMR spectrum of TCbzBz in CD₂Cl₂

References

1. B. W. D'Andrade, S. Datta, S. R. Forrest, P. Djurovich, E. Polikarpov and M. E. Thompson, *Org. Electron.*, 2005, **6**, 11.
2. P. I. Djurovich, E. I. Mayo, S. R. Forrest and M. E. Thompson, *Org. Electron.*, 2009, **10**, 515.
3. Md. N. Islam, D. Bhattacharjee, S. A. Hussain, *Chin. Phys. Lett.*, 2007, **24**, 2044-2047.
4. P. M. Robinson, H. G. Scott, *Mol. Cryst. Liq. Cryst.* 1969, **5**, 405-411.